AIAA SciTech Forum
9 - 13 January 2017, Grapevine, Texas
AIAA Guidance, Navigation, and Control Conference

Successive Convexification for Mars 6-DoF Powered Descent Landing Guidance

Michael Szmuk, Utku Eren, and Behçet Açıkmeşe
University of Washington, Seattle, WA 98195-2400

In this paper we propose an iterative successive convexification algorithm for the 6-DoF fixed-final-time fuel-optimal Mars powered descent landing guidance problem. We assume that the vehicle is actuated by a single gimbaled rocket motor with lower and upper thrust bounds, and that aerodynamic forces are negligible. Solving this problem in real-time is challenging for three reasons. First, it is non-convex due to its thrust-magnitude lower bound, mass-depletion dynamics, and attitude dynamics. Second, the consistency of attitude transformations is highly dependent on the magnitude of the attitude quaternion, thus making the accuracy of the problem discretization key. Third, the initialization of an iterative process can be challenging since a suitable reference trajectory is not readily available. Our algorithm addresses these issues in the following ways. First, we employ successive convexification to handle non-convexities. Second, we compute the linearized system's state and control matrices to ensure that upon convergence, the nonlinear dynamics are accurately satisfied. Lastly, we show that our algorithm can converge even when initialized with a very simple, dynamically inconsistent reference trajectory. Using the aforementioned techniques, our algorithm converts the original problem into a sequence of second-order cone programming (SOCP) problems that can be solved quickly and reliably using Interior Point Method (IPM) algorithms suitable for real-time autonomous applications.

Nomenclature

DoF	Degrees-of-Freedom
IPM	Interior Point Method
SC	Successive Convexification
SOCP	Second-Order Cone Programming
m	landing vehicle mass
m_{dry}	dry mass of the landing vehicle
m_{wet}	wet mass of the landing vehicle
$\mathbf{g}$	constant acceleration due to gravity
$\mathbf{T}_{\mathcal{B}}$	commanded thrust vector
α	constant of proportionality between thrust magnitude and mass consumption
$\mathbf{r}_{\mathcal{I}}$	landing vehicle's position
$\mathbf{v}_{\mathcal{I}}$	landing vehicle's velocity
$\mathbf{a}_{\mathcal{I}}$	landing vehicle's acceleration
$\mathbf{e}_{u,\mathcal{I}}$	Up-pointing unit vector in inertial frame
$C_{\mathcal{I}\leftarrow\mathcal{B}}$	direction-cosine-matrix from body to inertial frame
$\mathbf{g}_{\mathcal{I}}$	gravity vector in inertial frame
$q_{\mathcal{B}\leftarrow\mathcal{I}}$	quaternions defining rotation of the body relative to inertial frame
ξ	rotation angle component of quaternion
$\hat{\mathbf{v}}$	vector component of quaternion
q_i	elements of quaternion vector $q_{\mathcal{B}\leftarrow\mathcal{I}}$
$\boldsymbol{\omega}_{\mathcal{B}}$	angular velocity of landing vehicle relative to inertial frame
$\mathbf{r}_{CM,\mathcal{B}}$	center of mass of the landing vehicle
$J_{\mathcal{B}}$	moment of inertia of the landing vehicle
$\mathbf{r}_{T,\mathcal{B}}$	constant position vector of the engine gimbal point w.r.t. $\mathbf{r}_{CM,\mathcal{B}}$
γ_{gs}	glideslope constraint angle
θ	tilt angle of the landing vehicle
θ_{max}	maximum tilt angle
ω_{max}	maximum angular rate
δ_{max}	maximum gimbal angle
t	time
t_f	final time of the trajectory
x	full state vector of the landing vehicle
Φ_A	state transition matrix for the full state dynamics

I. Introduction

Powered-descent guidance problem has risen into prominence among both academic and industrial researchers due to the recent successes of missions to Mars and further long-term planned missions. The importance of powered-descent landing technology lies in its two key benefits for the future of space explorations: achieving unprecedented level of landing accuracy in planetary missions and providing a cost effective Earth-to-orbit access by enabling reusable launch vehicles. These benefits are already evidenced through successful landing of Mars Science Laboratory (MSL) on Mars in August of 2012, as well as concurrent development on multiple suborbital and orbital launch vehicles in the past decade.

The ability to perform a guided descent and landing brings along stringent challenges. More specifically, nonlinear dynamics of the landing vehicle coupled with various non-convex constraints renders the problem difficult to solve in real-time. Furthermore, sensitivity of mission availability depends on the efficient utilization of performance envelope i.e., success of the landing sequence is bounded by the ability to generate trajectories on the edges of physically feasible scenarios. Several insightful methods are proposed[1–3] to analytically obtain suboptimal guidance trajectory solutions. Although some requirements such as constraints on control, attitude and attitude rate[4] are incorporated, these analytical solutions were limited in terms of comprehensive set of mission and vehicle constraints. Recently, model predictive control has been used to address the powered-descent guidance and control problem.[5] Another approach uses a dual quaternion and model predictive control based powered-descent guidance and control method.[6,7] This method is capable of addressing mission requirements such as 6-DoF line of sight constraints. Essentially, the method utilizes piecewise affine approximations of the nonlinear rotational and translational rigid-body dynamics, and formulates the powered-descent problem in model predicted control framework with dual quaternions on convex representable subsets.

Deterministic convergence guarantees to the globally optimal solution[8] and availability of efficient interior point method (IPM) algorithms[9–12] feature convex optimization as a promising tool for onboard autonomy. To this end, by exploiting certain structures of the problem, a lossless convexification[13–15] based guidance algorithm is designed[16–20] and demonstrated[21,22] for precise powered-descent landing with non-convex control constraints. Although lossless convexification proved itself powerful, it may not be available in certain problem structures such as nonlinear kinematics or dynamics. Successive convexification gains research interest due to its capability to address nonlinear dynamics by transforming the non-convex problem into sequence of convex programming problems.[23–29] The successive convexification technique consists of repeatedly linearizing the problem around the previously obtained trajectory, and iterating until a user-defined convergence criteria is met. To facilitate convergence, two key components are introduced: quadratic trust regions to keep the solution bounded and a relaxation term to the dynamics to ensure feasibility throughout the convergence process.

In this paper we propose a successive convexification algorithm that is suitable for the guidance problem of 6-DoF fuel optimal Mars powered-descent landing. The algorithm is essentially an extension of our previous work[27] via incorporating attitude kinematics and decoupling the thrust vector from attitude of landing vehicle. The landing vehicle is actuated by a single gimbaled rocket motor with finite propellant and throttleable rocket engine has lower and upper thrust bounds along with maximum gimbal angle. Also, during its free final time descent, the vehicle is subject to safety related restrictions such as glide-slope, maximum tilt angle and angular rate constraints. The proposed method is not only suitable for real-time applications, but also capable of generating better performing feasible trajectories when compared to alternative heuristic guidance strategies, hence, making better use of the actual flight envelope.

The paper is organized as follows. In Section II, we state the continuous-time non-convex 6-DoF powered-descent landing problem. In Section III, we propose our modifications to recast the initial problem formulation as a convex optimization problem, and we give the full description of our successive convexification algorithm. Lastly, in Section IV, we present simulation results for a powered landing scenario to demonstrate the effectiveness of the proposed algorithm.

II. Problem Description

In this section, we state the non-convex minimum-fuel optimal control problem for a 6-DoF rocket powered Mars landing scenario. To make the problem more tractable, we will consider a fixed-final-time problem. Furthermore, for the remainder of this paper, we will use two reference frames:

(1) $\mathcal{F}_\mathcal{I}$: An inertially-fixed Up-East-North frame centered at the landing site.

(2) $\mathcal{F}_\mathcal{B}$: A body-fixed reference frame centered at the vehicle's center of mass, with its x-axis aligned with the thrust vector when the engine is not gimbaled, the y-axis pointing out the side of the vehicle, and the z-axis completing the right-handed system.

The remainder of this section will outline the dynamics and kinematics, and the state and control constraints inherent in the 6-DoF rocket landing problem. The section will conclude with a summary of the non-convex problem statement. Unless otherwise stated, the equations in this section apply over the time window $t \in [0, t_f]$, where t_f is a fixed final time.

II.A. Dynamics and Kinematics

During the powered descent phase of landing, the vehicle is assumed to be a rigid body subject to constant gravitational acceleration, g, and negligible aerodynamic forces. Without loss of generality, we will assume that the vehicle commands a single engine to produce a thrust vector within a feasible range of magnitudes and gimbal angles. In doing so, the vehicle depletes its mass, $m(t)$, at a rate proportional to the magnitude of the commanded thrust vector, $\mathbf{T}_\mathcal{B}(t)$.[17] The mass depletion dynamics are thus given by:

$$\dot{m}(t) = -\alpha \|\mathbf{T}_\mathcal{B}(t)\|_2 \tag{1}$$

We will denote the position, velocity, and acceleration of the vehicle in $\mathcal{F}_\mathcal{I}$ as $\mathbf{r}_\mathcal{I}(t)$, $\mathbf{v}_\mathcal{I}(t)$, and $\mathbf{a}_\mathcal{I}(t)$, respectively. Thus, we express the double-integrator dynamics of the vehicle as:

$$\dot{\mathbf{r}}_\mathcal{I}(t) = \mathbf{v}_\mathcal{I}(t) \tag{2a}$$
$$\dot{\mathbf{v}}_\mathcal{I}(t) = \mathbf{a}_\mathcal{I}(t) \tag{2b}$$

We will give an expression for $\mathbf{a}_\mathcal{I}(t)$ at the end of this section, after all of the parameters have been introduced. The attitude of $\mathcal{F}_\mathcal{B}$ relative to $\mathcal{F}_\mathcal{I}$ will be parametrized using unit quaternions, which we denote as:

$$q_{\mathcal{B}\leftarrow\mathcal{I}} = \begin{bmatrix} \cos(\xi/2) \\ \sin(\xi/2)\hat{\mathbf{v}} \end{bmatrix} = \begin{bmatrix} q_0 & q_1 & q_2 & q_3 \end{bmatrix}^T$$

We will denote the angular velocity vector of $\mathcal{F}_\mathcal{B}$ relative to $\mathcal{F}_\mathcal{I}$ as $\boldsymbol{\omega}_\mathcal{B}(t)$, and we will define $\Omega\big(\boldsymbol{\omega}_\mathcal{B}\big)$ as:

$$\Omega\big(\boldsymbol{\omega}_\mathcal{B}\big) \triangleq \begin{bmatrix} 0 & -\omega_x & -\omega_y & -\omega_z \\ \omega_x & 0 & \omega_z & -\omega_y \\ \omega_y & -\omega_z & 0 & \omega_x \\ \omega_z & \omega_y & -\omega_x & 0 \end{bmatrix}$$

Then, the attitude kinematics are given as follows:

$$\dot{q}_{\mathcal{B}\leftarrow\mathcal{I}}(t) = \frac{1}{2}\Omega\big(\boldsymbol{\omega}_\mathcal{B}(t)\big) q_{\mathcal{B}\leftarrow\mathcal{I}}(t) \tag{3a}$$
$$\dot{\boldsymbol{\omega}}_\mathcal{B}(t) = \boldsymbol{\alpha}_\mathcal{B}(t) \tag{3b}$$

To make the problem more tractable, we assume that the center of mass, $\mathbf{r}_{CM,\mathcal{B}}$, and the moment of inertia, $J_\mathcal{B}$, remain constant with respect to $\mathcal{F}_\mathcal{B}$. Since the origin of $\mathcal{F}_\mathcal{B}$ coincides with the center of mass, we denote the constant position vector of the engine gimbal point as $\mathbf{r}_{T,\mathcal{B}}$. Consequently, we express $\boldsymbol{\alpha}_\mathcal{B}(t)$ as:

$$\boldsymbol{\alpha}_\mathcal{B}(t) = J_\mathcal{B}^{-1}\Big(\left[\mathbf{r}_{T,\mathcal{B}}\times\right] \mathbf{T}_\mathcal{B}(t) - \left[\boldsymbol{\omega}_\mathcal{B}(t)\times\right] J_\mathcal{B}\boldsymbol{\omega}_\mathcal{B}(t) \Big) \tag{4}$$

Lastly, denoting the direction-cosine-matrix from $\mathcal{F}_\mathcal{B}$ to $\mathcal{F}_\mathcal{I}$ as $C_{\mathcal{I}\leftarrow\mathcal{B}}(t) \triangleq C_{\mathcal{I}\leftarrow\mathcal{B}}\big(q_{\mathcal{B}\leftarrow\mathcal{I}}(t)\big)$, and defining the gravity vector as $\mathbf{g}_\mathcal{I} \triangleq -g\mathbf{e}_{u,\mathcal{I}}$, we express $\mathbf{a}_\mathcal{I}(t)$ as follows:

$$\mathbf{a}_\mathcal{I}(t) = \frac{1}{m(t)} C_{\mathcal{I}\leftarrow\mathcal{B}}(t)\mathbf{T}_\mathcal{B}(t) + \mathbf{g}_\mathcal{I} \tag{5}$$

II.B. State and Control Constraints

We constrain the mass of the vehicle to be greater than the dry mass, m_{dry}, of the vehicle:

$$m_{dry} \leq m(t) \tag{6}$$

The path of the vehicle is constrained to stay above a cone with a minimum glide-slope angle $\gamma_{gs} \in [0^\circ, 90^\circ)$ above the horizon. This constraint is expressed as:

$$\begin{aligned} \mathbf{e}_{u,\mathcal{I}}^T \mathbf{r}_\mathcal{I}(t) &\geq \tan\gamma_{gs} \|H_{en}^T \mathbf{r}_\mathcal{I}(t)\|_2 \\ H_{en} &\triangleq \begin{bmatrix} \mathbf{e}_{e,\mathcal{I}} & \mathbf{e}_{n,\mathcal{I}} \end{bmatrix} \end{aligned} \tag{7}$$

We define the tilt angle of the vehicle, $\theta(t)$, as the angle between the x-axes of $\mathcal{F}_\mathcal{B}$ and $\mathcal{F}_\mathcal{I}$. Formally, this is expressed as:

$$\cos\theta(t) = \mathbf{e}_{u,\mathcal{I}} \cdot \mathbf{e}_{x,\mathcal{I}}(t) \tag{8a}$$

$$= \mathbf{e}_{u,\mathcal{I}}^T C_{\mathcal{I}\leftarrow\mathcal{B}}(t)\mathbf{e}_{x,\mathcal{B}} \tag{8b}$$

$$= 1 - 2[q_2^2(t) + q_3^2(t)] \tag{8c}$$

Note that the quaternion elements in Eq. (8) are elements of $q_{\mathcal{B}\leftarrow\mathcal{I}}(t)$. To avoid excessive tilt angles in the trajectory, we constrain the tilt angle to a maximum value of θ_{max}. Thus, we express the tilt constraint as:

$$\cos\theta_{max} \leq 1 - 2[q_2^2(t) + q_3^2(t)] \tag{9}$$

The angular rates of the vehicle are constrained to a maximum angular rate of ω_{max}:

$$\|\boldsymbol{\omega}_\mathcal{B}(t)\|_2 \leq \omega_{max} \tag{10}$$

The thrust magnitude is lower- and upper-bounded as follows:

$$T_{min} \leq \|\mathbf{T}_\mathcal{B}(t)\|_2 \leq T_{max} \tag{11}$$

Lastly, the gimbal angle is constrained to maximum angle of δ_{max} as follows:

$$\cos\delta_{max}\|\mathbf{T}_\mathcal{B}(t)\|_2 \leq \mathbf{e}_{u,\mathcal{B}}^T \mathbf{T}_\mathcal{B}(t) \tag{12}$$

II.C. Problem Statement

We now summarize the fixed-final-time non-convex rocket powered landing problem addressed in this paper. In this problem, we attempt to minimize the propellant used (i.e. maximize the final mass) subject to (a) boundary conditions, (b) the dynamics and kinematics in Eqs. (1)-(5), (c) the state constraints in Eqs. (6)-(7),(9)-(10), and (d) the control constraints in Eqs. (11)-(12). Problem 1 summarizes the problem statement.

Problem 1.

Cost Function:

$$\underset{\mathbf{T}_{\mathcal{B}}(t)}{\text{maximize}} \quad m(t_f)$$

subject to:

Boundary Conditions:

$$\begin{aligned}
m(0) &= m_{wet} \\
\mathbf{r}_{\mathcal{I}}(0) &= \mathbf{r}_{\mathcal{I},i} & \mathbf{r}_{\mathcal{I}}(t_f) &= \mathbf{r}_{\mathcal{I},f} \\
\mathbf{v}_{\mathcal{I}}(0) &= \mathbf{v}_{\mathcal{I},i} & \mathbf{v}_{\mathcal{I}}(t_f) &= \mathbf{v}_{\mathcal{I},f} \\
q_{\mathcal{B}\leftarrow\mathcal{I}}(0) &= q_{\mathcal{B}\leftarrow\mathcal{I},i} & q_{\mathcal{B}\leftarrow\mathcal{I}}(t_f) &= q_{\mathcal{B}\leftarrow\mathcal{I},f} \\
\boldsymbol{\omega}_{\mathcal{B}}(0) &= \boldsymbol{\omega}_{\mathcal{B},i} & \boldsymbol{\omega}_{\mathcal{B}}(t_f) &= \boldsymbol{\omega}_{\mathcal{B},f} \\
\mathbf{a}_{\mathcal{I}}(0) &= \mathbf{a}_{\mathcal{I},i} & \mathbf{a}_{\mathcal{I}}(t_f) &= \mathbf{a}_{\mathcal{I},f} \\
\boldsymbol{\alpha}_{\mathcal{B}}(0) &= \boldsymbol{\alpha}_{\mathcal{B},i} & \boldsymbol{\alpha}_{\mathcal{B}}(t_f) &= \boldsymbol{\alpha}_{\mathcal{B},f}
\end{aligned}$$

Dynamics:

$$\begin{aligned}
\dot{m}(t) &= -\alpha\|\mathbf{T}_{\mathcal{B}}(t)\|_2 \\
\dot{\mathbf{r}}_{\mathcal{I}}(t) &= \mathbf{v}_{\mathcal{I}}(t) \\
\dot{\mathbf{v}}_{\mathcal{I}}(t) &= \frac{1}{m(t)} C_{\mathcal{I}\leftarrow\mathcal{B}}(t)\mathbf{T}_{\mathcal{B}}(t) + \mathbf{g}_{\mathcal{I}} \\
\dot{q}_{\mathcal{B}\leftarrow\mathcal{I}}(t) &= \Omega\big(\boldsymbol{\omega}_{\mathcal{B}}(t)\big) q_{\mathcal{B}\leftarrow\mathcal{I}}(t) \\
\dot{\boldsymbol{\omega}}_{\mathcal{B}}(t) &= J_{\mathcal{B}}^{-1}\Big(\left[\mathbf{r}_{T,\mathcal{B}}\times\right] \mathbf{T}_{\mathcal{B}}(t) - \left[\boldsymbol{\omega}_{\mathcal{B}}(t)\times\right] J_{\mathcal{B}}\boldsymbol{\omega}_{\mathcal{B}}(t) \Big)
\end{aligned}$$

State Constraints:

$$\begin{aligned}
m_{dry} &\leq m(t) \\
\tan\gamma_{gs}\|H_{en}^T\mathbf{r}_{\mathcal{I}}(t)\|_2 &\leq \mathbf{e}_{u,\mathcal{I}}^T\mathbf{r}_{\mathcal{I}}(t) \\
\cos\theta_{max} &\leq 1 - 2[q_2^2(t) + q_3^2(t)] \\
\|\boldsymbol{\omega}_{\mathcal{B}}(t)\|_2 &\leq \omega_{max}
\end{aligned}$$

Control Constraints:

$$\begin{aligned}
T_{min} \leq \|\mathbf{T}_{\mathcal{B}}(t)\|_2 &\leq T_{max} \\
\cos\delta_{max}\|\mathbf{T}_{\mathcal{B}}(t)\|_2 &\leq \mathbf{e}_{u,\mathcal{B}}^T\mathbf{T}_{\mathcal{B}}(t)
\end{aligned}$$

III. Convex Formulation

We now seek to re-formulate Problem 1 in a way that leverages powerful convex optimization algorithms. Specifically, we will linearize and discretize Problem 1 to produce a sequence of second-order cone programming problems that will be solved successively to convergence, a process we call *successive convexification*.

This section is organized as follows. Sections III.A-III.C outline the steps required to re-formulate Problem 1 within the successive convexification framework. Section III.D.1 gives a summary of the second-order cone programming problem formulation, and discusses the addition of trust regions and dynamics relaxations. Section III.D.2 will give a description of the successive convexification algorithm.

III.A. Decoupling States and Controls

In our work, we found that the linearization of the non-convex optimal control problem resulted in high-frequency chatter in the control variable, $\mathbf{T}_{\mathcal{B}}(t)$. This is a phenomenon that has been observed in related work.[25,28] Specifically, the cause of the high-frequency chatter is believed to be caused by the nonlinear coupling of state and control constraints.[28] As such, we seek to decouple the state and control variables by, instead, controlling the second derivative of $\mathbf{T}_{\mathcal{B}}(t)$, which we denote as $u(t) \in \mathbb{R}^3$. Thus, we form the

following system of integrators:

$$\frac{d}{dt}\mathbf{T}_{\mathcal{B}}(t) = \dot{\mathbf{T}}_{\mathcal{B}}(t) \tag{13a}$$

$$\frac{d}{dt}\dot{\mathbf{T}}_{\mathcal{B}}(t) = u(t) \tag{13b}$$

Consequently, $\mathbf{T}_{\mathcal{B}}(t)$ and $\dot{\mathbf{T}}_{\mathcal{B}}(t)$ become state variables, and $u(t)$ becomes the new control variable. The implication of the latter is that the control matrix $B(t)$ becomes a constant matrix. That is:

$$B \triangleq B(t) \quad \forall t \in [0, t_f] \tag{14}$$

In our experience, this modification produced smoother thrust profiles, and provided the additional benefit of increasing the feasibility envelope of the problem by increasing the level of control between time sample points. Note that aside from the bounds imposed on $\mathbf{T}_{\mathcal{B}}(t)$ in Eqs. 11 and 12, no additional constraints were placed on $\mathbf{T}_{\mathcal{B}}(t)$, $\dot{\mathbf{T}}_{\mathcal{B}}(t)$, and $u(t)$. Therefore, our convex formulation has state constraints, but does not include any control constraints.

III.B. Linearization

III.B.1. Dynamics

To simplify our notation, we will now define the state vector $x(t) \in \mathbb{R}^{20}$ as follows:

$$x(t) = \begin{bmatrix} m(t) & \mathbf{r}_{\mathcal{I}}(t) & \mathbf{v}_{\mathcal{I}}(t) & q_{\mathcal{B}\leftarrow\mathcal{I}}(t) & \boldsymbol{\omega}_{\mathcal{B}}(t) & \mathbf{T}_{\mathcal{B}}(t) & \dot{\mathbf{T}}_{\mathcal{B}}(t) \end{bmatrix}^T \tag{15}$$

Note that Eq. 15 includes the state augmentation introduced in Section III.A. Next, we will express the augmented dynamics as a function of the augmented state:

$$\dot{x}(t) = f\big(x(t), u(t)\big) \triangleq \begin{bmatrix} -\alpha\|\mathbf{T}_{\mathcal{B}}(t)\|_2 \\ \mathbf{v}_{\mathcal{I}}(t) \\ \dfrac{1}{m(t)} C_{\mathcal{I}\leftarrow\mathcal{B}}(t)\mathbf{T}_{\mathcal{B}}(t) + \mathbf{g}_{\mathcal{I}} \\ \Omega\big(\boldsymbol{\omega}_{\mathcal{B}}(t)\big) q_{\mathcal{B}\leftarrow\mathcal{I}}(t) \\ J_{\mathcal{B}}^{-1}\Big(\left[\mathbf{r}_{T,\mathcal{B}}\times\right] \mathbf{T}_{\mathcal{B}}(t) - \left[\boldsymbol{\omega}_{\mathcal{B}}(t)\times\right] J_{\mathcal{B}}\boldsymbol{\omega}_{\mathcal{B}}(t)\Big) \\ \dot{\mathbf{T}}_{\mathcal{B}}(t) \\ u(t) \end{bmatrix} \tag{16}$$

When formulated in the context of a parameter optimization problem, Eq. 16 constitutes a set of non-convex equality constraints. To circumvent this issue, we replace the right hand side of Eq. 16 with a first-order Taylor series approximation of $f\big(x(t), u(t)\big)$, and will adopt the following notation:

$$\dot{x}(t) = A(t)x(t) + B(t)u(t) + z(t) \tag{17a}$$

$$A(t) \triangleq \frac{\partial f(x,u)}{\partial x}\Big|_{\substack{\bar{x}(t) \\ \bar{u}(t)}} \tag{17b}$$

$$B(t) \triangleq \frac{\partial f(x,u)}{\partial x}\Big|_{\substack{\bar{x}(t) \\ \bar{u}(t)}} \tag{17c}$$

$$z(t) \triangleq f\big(\bar{x}(t), \bar{u}(t)\big) - A(t)\bar{x}(t) - B(t)\bar{u}(t) \tag{17d}$$

III.B.2. State Constraints

Problem 1 has a number of non-convex state and control constraints. Specifically, these consist of the boundary conditions on $\mathbf{a}_\mathcal{I}$ and $\boldsymbol{\alpha}_\mathcal{B}$, and Eq. 11. Our approach is to directly linearize $\mathbf{a}_\mathcal{I}(t)$ and $\boldsymbol{\alpha}_\mathcal{B}(t)$ at the initial time and final time, and $\|\mathbf{T}_\mathcal{B}(t)\|_2$ about $\bar{x}(t)$. In doing so, we define the following functions:

$$f_{\mathbf{a}_\mathcal{I},t} \triangleq \bar{\mathbf{a}}_\mathcal{I}(t) + \left(\frac{\partial \mathbf{a}_\mathcal{I}}{\partial x}\Big|_{\bar{x}(t)}\right)\big(x(t) - \bar{x}(t)\big) \tag{18a}$$

$$f_{\boldsymbol{\alpha}_\mathcal{B},t} \triangleq \bar{\boldsymbol{\alpha}}_\mathcal{B}(t) + \left(\frac{\partial \boldsymbol{\alpha}_\mathcal{B}}{\partial x}\Big|_{\bar{x}(t)}\right)\big(x(t) - \bar{x}(t)\big) \tag{18b}$$

$$f_{\mathbf{T}_\mathcal{B},t} \triangleq \|\bar{\mathbf{T}}_\mathcal{B}(t)\|_2 + \left(\frac{\bar{\mathbf{T}}_\mathcal{B}^T(t)}{\|\bar{\mathbf{T}}_\mathcal{B}(t)\|_2}\right)\big(\mathbf{T}_\mathcal{B}(t) - \bar{\mathbf{T}}_\mathcal{B}(t)\big) \tag{18c}$$

Note that in Eqs. 18, $\bar{\mathbf{a}}_\mathcal{I}(t)$, $\bar{\boldsymbol{\alpha}}_\mathcal{B}(t)$, and $\bar{\mathbf{T}}_\mathcal{B}(t)$ are the values of $\mathbf{a}_\mathcal{I}(t)$, $\boldsymbol{\alpha}_\mathcal{B}(t)$, and $\mathbf{T}_\mathcal{B}(t)$, respectively, about which the equations are linearized.

III.C. Discretization

To cast the continuous-time optimal control problem into a finite-dimensional parameter optimization problem, we discretize the trajectory at K points in time. Denoting the final time of the trajectory as t_f, we define the time at index $k \in \mathbb{Z}$ as:

$$t_k \triangleq \left(\frac{k}{K-1}\right) t_f, \quad k \in [0, K)$$

We assume a first-order-hold on the control, $u(t)$, over each time step. Consequently, $u(t)$ can be written in terms of $u_k \triangleq u(t_k)$ and $u_{k+1} \triangleq u(t_{k+1})$ over $k \in [0, K)$ as follows:

$$u(t) = \lambda_k^-(t) u_k + \lambda_k^+(t) u_{k+1} \tag{19a}$$

$$\lambda_k^-(t) \triangleq \left(\frac{t_{k+1} - t}{t_{k+1} - t_k}\right) \tag{19b}$$

$$\lambda_k^+(t) \triangleq \left(\frac{t - t_k}{t_{k+1} - t_k}\right) \tag{19c}$$

Furthermore, we use $\Phi_A(t_{k+1}, t_k)$ to denote the state transition matrix that describes the zero-input evolution from x_k to x_{k+1}, and that is governed by the matrix differential equation:

$$\frac{d}{dt}\Phi_A(t, t_k) = A(t)\Phi_A(t, t_k), \quad \Phi_A(t_k, t_k) = I \tag{20}$$

Using Eqs. 14, 19, and 20, we express the discrete-time dynamics that relate $x_k \triangleq x(t_k)$ to $x_{k+1} \triangleq x(t_{k+1})$ over $k \in [0, K)$ as follows:

$$x_{k+1} = \tilde{A}_k x_k + \tilde{B}_k^- u_k + \tilde{B}_k^+ u_{k+1} + \tilde{z}_k \tag{21a}$$

$$\tilde{A}_k \triangleq \Phi_A(t_{k+1}, t_k) \tag{21b}$$

$$\tilde{B}_k^- \triangleq \tilde{A}_k \int_{t_k}^{t_{k+1}} \lambda_k^-(\tau)\Phi_A(t_k, \tau)B d\tau \tag{21c}$$

$$\tilde{B}_k^+ \triangleq \tilde{A}_k \int_{t_k}^{t_{k+1}} \lambda_k^+(\tau)\Phi_A(t_k, \tau)B d\tau \tag{21d}$$

$$\tilde{z}_k \triangleq \tilde{A}_k \int_{t_k}^{t_{k+1}} \Phi_A(t_k, \tau)z(\tau) d\tau \tag{21e}$$

Lastly, in the discretized parameter optimization problem, the state and control constraints from Problem 1 are enforced at discrete time instances t_k, with $k \in [0, K]$.

III.D. Successive Convexification

III.D.1. Problem Formulation

In this section, we state the second-order cone programming problem that is at the core of our successive convexification algorithm. Once initialized, our algorithm solves this parameter optimization problem repeatedly to arrive at a converged solution. However, due to linearization, we must take precautions to avoid artificially rendering the problem unbounded or infeasible. As such, we introduce two additional modifications[26,27] alongside those discussed in Sections III.A-III.C.

First, we add quadratic trust regions to ensure that the problem remains bounded. These trust regions also ensure that the solution remains close to the linearization point, thus aiding in numerical stability throughout the solution process. To proceed, we define $\delta x_k \triangleq x_k - \bar{x}_k$ and $\delta u_k \triangleq u_k - \bar{u}_k$, and introduce a new variable $\eta \in \mathbb{R}^K$, where we denote the k^{th} element of η as η_k. We express the trust region using the following convex inequality constraint:

$$\delta x_k^T \delta x_k + \delta u_k^T \delta u_k \leq \eta_k \tag{22}$$

To bound the size of the trust regions, we augment the original objective function with $w_\eta \|\eta\|_2$, where $w_\eta \in \mathbb{R}_{++}$.

Second, we relax the discrete-time dynamics given in Eq. 21a to prevent artificial infeasibility. We do this by introducing variables $\nu_k \in \mathbb{R}^{20}$ for $k \in [0, K)$, and $\kappa \in \mathbb{R}^{K-1}$, where we denote the k^{th} element of κ as κ_k. The relaxation of the dynamics is given by:

$$x_{k+1} = \tilde{A}_k x_k + \tilde{B}_k^- u_k + \tilde{B}_k^+ u_{k+1} + \tilde{z}_k + \nu_k \tag{23a}$$

$$\|\nu_k\|_2 \leq \kappa_k \tag{23b}$$

The intent of this relaxation is to allow deviation from the proper dynamics when infeasibility is unavoidable on a given iteration (e.g. due to the linearization point $\bar{x}$ and $\bar{u}$). To prevent such deviations from occurring when a feasible solution exists, we augment the objective function with $w_\kappa \|\kappa\|_2$, where $w_\kappa \in \mathbb{R}_{++}$ is a large weight.

Lastly, before we present the final problem statement, we rearrange Eq. 9 into a more canonical form. Since in our formulation we assume $q_{\mathcal{B}\leftarrow\mathcal{I},k} \in \mathbb{R}^4$, we can rewrite Eq. 9 as follows over $k \in [0, K]$:

$$\|H_q q_{\mathcal{B}\leftarrow\mathcal{I},k}\|_2 \leq \sqrt{\frac{1-\cos\theta_{max}}{2}} \tag{24a}$$

$$H_q \triangleq \begin{bmatrix} 0 & 0 & 1 & 0 \\ 0 & 0 & 0 & 1 \end{bmatrix} \tag{24b}$$

The remainder of the non-convexities found in the state and control constraints of Problem 1 were linearized in Eqs. 18. The summary of the convex formulation is provided in Problem 2 in the form of a second-order cone programming problem.

Problem 2.

Cost Function:

$$\underset{u_k}{\text{minimize}} \quad -m_K + w_\eta\|\eta\|_2 + w_\kappa\|\kappa\|_2$$

subject to:

Boundary Conditions:

$$\begin{aligned}
m_0 &= m_{wet} \\
\mathbf{r}_{\mathcal{I},0} &= \mathbf{r}_{\mathcal{I},i} & \mathbf{r}_{\mathcal{I},K} &= \mathbf{r}_{\mathcal{I},f} \\
\mathbf{v}_{\mathcal{I},0} &= \mathbf{v}_{\mathcal{I},i} & \mathbf{v}_{\mathcal{I},K} &= \mathbf{v}_{\mathcal{I},f} \\
q_{\mathcal{B}\leftarrow\mathcal{I},0} &= q_{\mathcal{B}\leftarrow\mathcal{I},i} & q_{\mathcal{B}\leftarrow\mathcal{I},K} &= q_{\mathcal{B}\leftarrow\mathcal{I},f} \\
\boldsymbol{\omega}_{\mathcal{B},0} &= \boldsymbol{\omega}_{\mathcal{B},i} & \boldsymbol{\omega}_{\mathcal{B},K} &= \boldsymbol{\omega}_{\mathcal{B},f} \\
f_{\mathbf{a}_\mathcal{I},0} &= \mathbf{a}_{\mathcal{I},i} & f_{\mathbf{a}_\mathcal{I},K} &= \mathbf{a}_{\mathcal{I},f} && \text{(see Eq. 18a)} \\
f_{\boldsymbol{\alpha}_\mathcal{B},0} &= \boldsymbol{\alpha}_{\mathcal{B},i} & f_{\boldsymbol{\alpha}_\mathcal{B},K} &= \boldsymbol{\alpha}_{\mathcal{B},f} && \text{(see Eq. 18b)}
\end{aligned}$$

Dynamics:

$$x_{k+1} = \tilde{A}_k x_k + \tilde{B}_k^- u_k + \tilde{B}_k^+ u_{k+1} + \tilde{z}_k + \nu_k \quad \text{(see Eqs. 15-21, 23a)}$$

State Constraints:

$$\begin{aligned}
m_{dry} &\leq m_k \\
\tan\gamma_{gs}\|H_{en}^T\mathbf{r}_{\mathcal{I},k}\|_2 &\leq \mathbf{e}_{u,\mathcal{I}}^T\mathbf{r}_{\mathcal{I},k} \\
\|H_q q_{\mathcal{B}\leftarrow\mathcal{I},k}\|_2 &\leq \sqrt{\frac{1-\cos\theta_{max}}{2}} && \text{(see Eqs. 24)} \\
\|\boldsymbol{\omega}_{\mathcal{B},k}\|_2 &\leq \omega_{max} \\
T_{min} \leq f_{\mathbf{T}_\mathcal{B},k} &\leq T_{max} && \text{(see Eq. 18c)} \\
\cos\delta_{max}\|\mathbf{T}_{\mathcal{B},k}\|_2 &\leq \mathbf{e}_{u,\mathcal{B}}^T\mathbf{T}_{\mathcal{B},k}
\end{aligned}$$

Trust Region:

$$\delta x_k^T\delta x_k + \delta u_k^T\delta u_k \leq \eta_k \quad \text{(see Eq. 22)}$$

Dyn. Relaxation:

$$\|\nu_k\|_2 \leq \kappa_k \quad \text{(see Eqs. 23b)}$$

III.D.2. Algorithm

We now present the successive convexification algorithm. Algorithm 1 outlines the successive convexification procedure, including the method by which to initialize the algorithm. Note that the initialization trajectory does not satisfy the nonlinear dynamics in Eq. 16, and thus is not dynamically consistent.

Algorithm 1.

Initialization:

for $k \in [0, K]$:

$$\bar{m}_k = \left(\frac{K-k}{K}\right) m_{wet} + \left(\frac{k}{K}\right) m_{dry}$$
$$\bar{\mathbf{r}}_{\mathcal{I},k} = \left(\frac{K-k}{K}\right) \mathbf{r}_{\mathcal{I},i} + \left(\frac{k}{K}\right) \mathbf{r}_{\mathcal{I},f}$$
$$\bar{\mathbf{v}}_{\mathcal{I},k} = \left(\frac{K-k}{K}\right) \mathbf{v}_{\mathcal{I},i} + \left(\frac{k}{K}\right) \mathbf{v}_{\mathcal{I},f}$$
$$\bar{q}_{\mathcal{B}\leftarrow\mathcal{I},k} = \begin{bmatrix} 1 & 0 & 0 & 0 \end{bmatrix}^T$$
$$\bar{\mathbf{T}}_{\mathcal{B},k} = \bar{m}_k g \mathbf{e}_{u,\mathcal{I}}$$

Set $\bar{x}_k^{(0)} = \begin{bmatrix} \bar{m}_k^T & \bar{\mathbf{r}}_{\mathcal{I},k}^T & \bar{\mathbf{v}}_{\mathcal{I},k}^T & \bar{q}_{\mathcal{B}\leftarrow\mathcal{I},k}^T & \mathbf{0} & \bar{\mathbf{T}}_{\mathcal{B},k}^T & \mathbf{0} \end{bmatrix}^T$ and $\bar{u}_k^{(0)} = \mathbf{0}$

end

for $k \in [0, K)$:

Compute $\tilde{A}_k^{(0)}$, $\tilde{B}_k^{-,(0)}$, $\tilde{B}_k^{+,(0)}$, and $\tilde{z}_k^{(0)}$ using Eqs. 19-21

end

Successive Convexification Loop:

for $i \in [1, i_{max})$

(1) Using $\bar{x}_k^{(i-1)}$, $\bar{u}_k^{(i-1)}$, $\tilde{A}_k^{(i-1)}$, $\tilde{B}_k^{-,(i-1)}$, $\tilde{B}_k^{+,(i-1)}$, and $\tilde{z}_k^{(i-1)}$, solve Problem 2 to obtain $x_k^{(i)}$ and $u_k^{(i)}$

(2) Set $x_k^{(i)} \rightarrow \bar{x}_k^{(i)}$, $u_k^{(i)} \rightarrow \bar{u}_k^{(i)}$

(3) Compute $\tilde{A}_k^{(i)}$, $\tilde{B}_k^{-,(i)}$, $\tilde{B}_k^{+,(i)}$, and $\tilde{z}_k^{(i)}$ using Eqs. 19-21

(4) if $\|\eta^{(i)}\|_2 \leq$ tol

exit loop

end if

IV. Simulation Results

In this section we present simulation results that demonstrate our algorithm. Tables 1 and 2 present the simulation and algorithm parameters used in the simulation. In this example, the vehicle begins above and to the east of the landing site. The vehicle's initial velocity is downwards and to the north, its initial attitude is vertical, and its initial angular rate and accelerations are zero. The vehicle is required to land at the origin, with a downward velocity, a vertical attitude, and zero angular rate and accelerations.

Table 1. Simulation Parameters

Parameter	Value	Units
g	1	–
m_{dry}	0.75	–
T_{min}	0.5	–
T_{max}	4	–
δ_{max}	20	$^\circ$
θ_{max}	45	$^\circ$
γ_{gs}	10	$^\circ$
ω_{max}	100	$^\circ/s$
$J_{\mathcal{B}}$	diag([1 1 1])	–
α	0.10	–
$\mathbf{r}_{T,\mathcal{B}}$	[-1 0 0]^T	–

Table 2. B.C.'s and Algorithm Parameters

Parameter	Value	Units
t_f	6	–
m_{wet}	2.0	–
$\mathbf{r}_{\mathcal{I},i}$	[1 1 0]^T	–
$\mathbf{r}_{\mathcal{I},f}$	[0 0 0]^T	–
$\mathbf{v}_{\mathcal{I},i}$	[-0.2 0.0 0.1]^T	–
$\mathbf{v}_{\mathcal{I},f}$	[-0.1 0.0 0.0]^T	–
$q_{\mathcal{B}\leftarrow\mathcal{I},i}$, $q_{\mathcal{B}\leftarrow\mathcal{I},f}$	[1 0 0 0]^T	–
$\boldsymbol{\omega}_{\mathcal{B},i}$, $\boldsymbol{\omega}_{\mathcal{B},f}$	[0 0 0]^T	$^\circ/s$
$\mathbf{a}_{\mathcal{I},i}$, $\mathbf{a}_{\mathcal{I},f}$	[0 0 0]^T	–
$\boldsymbol{\alpha}_{\mathcal{B},i}$, $\boldsymbol{\alpha}_{\mathcal{B},f}$	[0 0 0]^T	–
K	30	–
i_{max}	10	–
w_η	1	–
w_κ	1×10^4	–

Figure 1 shows north-looking, west-looking, and down-looking views of the 3D trajectory produced by the last iteration of our algorithm. Evident in the solution is the non-minimum-phase behavior of the vehicle. For example, at the beginning of the trajectory, we see the vehicle travel east before reversing its velocity to the west. Likewise, at the end of the trajectory, the vehicle is seen to overshoot the landing site to the west before reversing its velocity to the east.

Figure 2 shows the thrust magnitude and gimbal angle history of the trajectory. As can be seen, the gimbal angle swings close to its maximum value a number of times as the vehicle changes its attitude. Meanwhile, the thrust oscillates smoothly and gently decreases over time, as the vehicle's mass is diminished throughout the trajectory.

V. Conclusion

In this paper, we presented a successive convexification algorithm that can be used to generate trajectories for a fixed-final-time 6-DoF Mars rocket powered landing. Our solution strategy for solving this non-convex optimal control problem consisted of solving a sequence of convex parameter optimization problems. Each parameter optimization problem was derived from the original non-convex problem formulation, and linearized about the previous trajectory. The iterative process was initialized using minimal a-priori knowledge of the trajectory, and results were presented to show that convergence can be attained under such starting conditions. The iterative process typically converges after solving less than ten second-order cone programming problems. Through the use of powerful IPM solvers, this algorithm is well suited for real time autonomous applications.

Acknowledgments

Support for developing the theoretical basis of the successive convexification method was provided by the National Science Foundation grant CNS-1446520 and the Office of Naval Research grant N00014-14-1-0314.

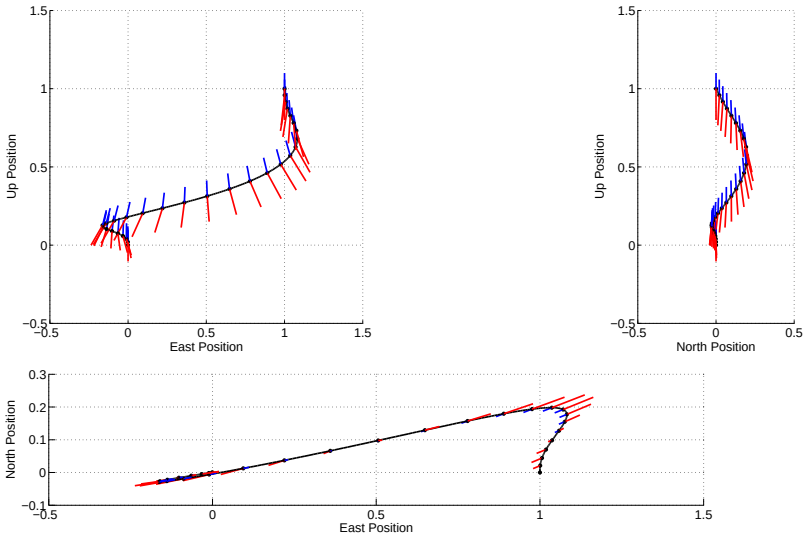

Figure 1. The converged solution of the three-dimensional trajectory landing trajectory. *The dots along the trajectory indicate discretization points, the red lines intersecting the trajectory at the discretization points represent scaled commanded thrust vectors, and the blue lines intersecting the trajectory represent the x-axis of the vehicle.*

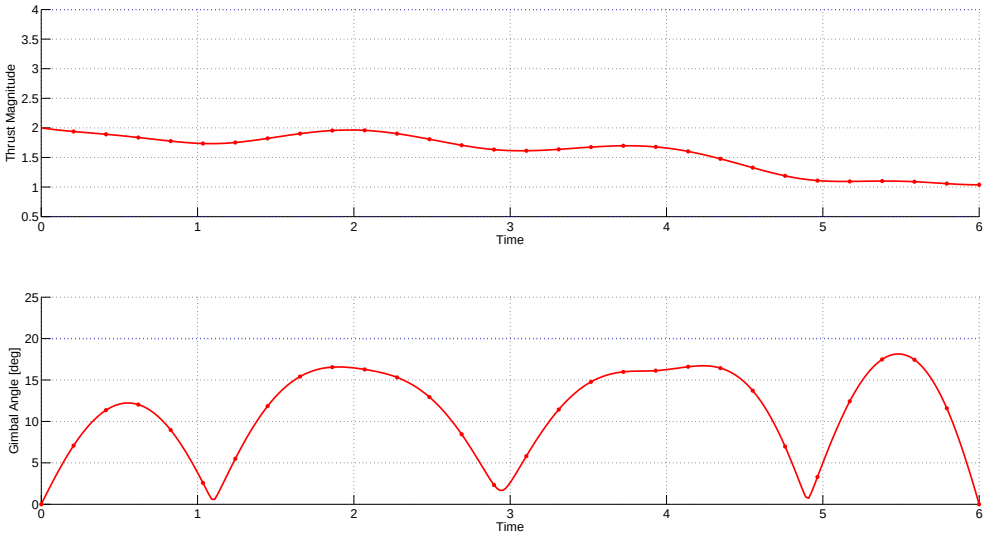

Figure 2. The converged solution of the thrust magnitude and gimbal angle. *The dotted blue lines represent the minimum and maximum thrusts, and the maximum allowed gimbal angle.*

References

[1]Klumpp, A. R., "Apollo Lunar Descent Guidance," *Automatica*, Vol. 10, 1974, pp. 133–146.

[2]Najson, F. and Mease, K. D., "Computationally Inexpensive Guidance Algorithm for Fuel-Efficient Terminal Descent," *Journal of Guidance, Control, and Dynamics*, Vol. 29, No. 4, 2006, pp. 955–964.

[3]Topcu, U., Casoliva, J., and Mease, K. D., "Minimum-Fuel Powered Descent for Mars Pinpoint Landing," *Journal of Spacecraft and Rockets*, Vol. 44, No. 2, 2007, pp. 324–331.

[4]Sostaric, R. R. and Rea, J. R., "Powered descent guidance methods for the moon and mars," *AIAA Guidance, Navigation, and Control Conference, San Francisco, CA*, 2005.

[5]Pascucci, C. A., Bennani, S., and Bemporad, A., "Model predictive control for powered descent guidance and control," *IEEE ECC Control Conference*, Linz, Austria, 07 2015.

[6]Lee, U. and Mesbahi, M., "Optimal Power Descent Guidance with 6-DoF Line of Sight Constraints via Unit Dual Quaternions," *AIAA SciTech, Guidance, Navigation, and Control*, Kissimmee, FL, 01/2015 2015.

[7]Lee, U. and Mesbahi, M., "Constrained Autonomous Precision Landing via Dual Quaternions and Model Predictive Control," *Journal of Guidance, Control, and Dynamics*, 2016.

[8]Boyd, S. and Vandenberghe, L., *Convex Optimization*, Cambridge University Press, 2004.

[9]Dueri, D., Zhang, J., and Açıkmeşe, B., "Automated Custom Code Generation for Embedded, Real-time Second Order Cone Programming," *IFAC World Congress*, 2014.

[10]Dueri, D., Açıkmeşe, B., Scharf, D. P., and Harris, M. W., "Customized Real-Time Interior-Point Methods for Onboard Powered-Descent Guidance," *Journal of Guidance, Control, and Dynamics*, 2016, pp. 1–16.

[11]Grant, M. and Boyd, S., "CVX: Matlab Software for Disciplined Convex Programming, version 2.1," *http://cvxr.com/cvx*, March 2014.

[12]Domahidi, A., Zgraggen, A. U., Zeilinger, M. N., Morari, M., and Jones, C. N., "Efficient interior point methods for multistage problems arising in receding horizon control," *Decision and Control (CDC), 2012 IEEE 51st Annual Conference on*, IEEE, 2012, pp. 668–674.

[13]Açıkmeşe, B. and Blackmore, L., "Lossless Convexification of a Class of Optimal Control Problems with Non-Convex Control Constraints," *Automatica*, Vol. 47, No. 2, 2011, pp. 341–347.

[14]Harris, M. and Açıkmeşe, B., "Lossless Convexification of Non-convex Optimal Control Problems for State Constrained Linear Systems," *Automatica*, Vol. 50, No. 9, 2014, pp. 2304–2311.

[15]Blackmore, L., Açıkmeşe, B., and Carson, J. M., "Lossless convexfication of control constraints for a class of nonlinear optimal control problems," *System and Control Letters*, Vol. 61, No. 4, 2012, pp. 863–871.

[16]Açıkmeşe, B. and Ploen, S. R., "A powered descent guidance algorithm for Mars pinpoint landing," *AIAA GNC Conference and Exhibit, San Francisco*, 2005.

[17]Açıkmeşe, B. and Ploen, S. R., "Convex Programming Approach to Powered Descent Guidance for Mars Landing," *AIAA Journal of Guidance, Control and Dynamics*, Vol. 30, No. 5, 2007, pp. 1353–1366.

[18]Blackmore, L., Açıkmeşe, B., and Scharf, D. P., "Minimum Landing Error Powered Descent Guidance for Mars Landing using Convex Optimization," *AIAA Journal of Guidance, Control and Dynamics*, Vol. 33, No. 4, 2010.

[19]Açıkmeşe, B., Carson, J., and Blackmore, L., "Lossless Convexification of Non-convex Control Bound and Pointing Constraints of the Soft Landing Optimal Control Problem," *IEEE Transactions on Control Systems Technology*, Vol. 21, No. 6, 2013, pp. 2104–2113.

[20]Harris, M. W. and Açıkmeşe, B., "Maximum Divert for Planetary Landing Using Convex Optimization," *Journal of Optimization Theory and Applications*, 2013, pp. 1–21.

[21]Açıkmeşe, B., Aung, M., Casoliva, J., Mohan, S., Johnson, A., Scharf, D., Masten, D., Scotkin, J., Wolf, A., and Regehr, M. W., "Flight Testing of Trajectories Computed by G-FOLD: Fuel Optimal Large Divert Guidance Algorithm for Planetary Landing," *AAS/AIAA Spaceflight Mechanics Meeting*, 2013.

[22]Scharf, D. P., M. W. Regehr, D. D., Açıkmeşe, B., Vaughan, G. M., Benito, J., Ansari, H., M. Aung, A. J., Masten, D., Nietfeld, S., Casoliva, J., and Mohan, S., "ADAPT Demonstrations of Onboard Large-Divert Guidance with a Reusable Launch Vehicle," *IEEE Aerospace Conference*, 2014.

[23]Casoliva, J., *Spacecraft Trajectory Generation by Successive Approximation for Powered Descent and Cyclers*, Ph.D. thesis, University of California, Irvine, 2013.

[24]Liu, X. and Lu, P., "Solving Nonconvex Optimal Control Problems by Convex Optimization," *Journal of Guidance, Control, and Dynamics*, Vol. 37, No. 3, 2014, pp. 750–765.

[25]Liu, X., Shen, Z., and Lu, P., "Entry trajectory optimization by second-order cone programming," *Journal of Guidance, Control, and Dynamics*, Vol. 39, No. 2, 2015, pp. 227–241.

[26]Mao, Y., Szmuk, M., and Acikmese, B., "Successive Convexification of Non-Convex Optimal Control Problems and Its Convergence Properties," *arXiv preprint arXiv:1608.05133*, 2016.

[27]Szmuk, M., Açıkmeşe, B., and Berning, A. W., "Successive Convexification for Fuel-Optimal Powered Landing with Aerodynamic Drag and Non-Convex Constraints," *AIAA SciTech, Guidance, Navigation, and Control*, San Diego, CA, 01/2016 2016.

[28]Wang, Z. and Grant, M. J., "Constrained Trajectory Optimization for Planetary Entry via Sequential Convex Programming," *AIAA Atmospheric Flight Mechanics Conference*, 2016, p. 3241.

[29]Liu, X. and Lu, P., "Solving nonconvex optimal control problems by convex optimization," *Journal of Guidance, Control, and Dynamics*, Vol. 37, No. 3, 2014, pp. 750–765.